CHIN. PHYS. LETT. Vol. 33, No. 6 (2016) 065201

Mega-Electron-Volt Electron Scattering and Radiography of Plasma *

Xue-Juan Wu(吴雪娟), Xiao-Fang Wang(王晓方)**, Xiao-Hu Chen(陈晓虎)
Department of Modern Physics, University of Science and Technology of China, Hefei 230026

(Received 7 January 2016)

A Monte Carlo code is developed to study mega-electron-volt (MeV) electron scattering and transport in plasma based on multiple scattering. A scaling law relating the angular width of a scattered beam to the incident electron energy and the areal density of plasma is found, which may provide a method of MeV electron radiography for diagnosing the areal density of high-temperature, dense plasma under fusion conditions. The study on the MeV electron beam radiography also shows that plasma density interfaces could be discriminated by electron scattering.

PACS: 52.25.Tx, 52.65.Pp, 52.70.−m DOI: 10.1088/0256-307X/33/6/065201

Since electron acceleration by a laser wakefield was proposed in 1979,[1] great progress has been made. Quasi-monoenergetic electron beams with several percent energy spread can be stably generated, typically in energy of hundreds of MeV, beam divergence less than 10 mrad, and pulse duration less than 100 fs.[2−4] Recently, GeV electron beams have been generated,[5,6] and the energy spread has reached less than a few percent.[6]

In view of advantages of MeV electron beams such as small source size, quasi-monoenergy, short duration, and temporal synchronization with the laser pulse, such a beam will meet broad applications in probing matter and dynamics. One is that a fast temporal resolution is expected for the diagnosis of electromagnetic fields by deflectometry.[7−12] For example, in 2013 Schumaker *et al.* used an electron beam of energy nearly 100 MeV to probe the magnetic field generated in laser–solid interactions and realized femtosecond temporal resolution.[12] On the other hand, an MeV electron beam has a deeper penetration in materials and can be applied for radiography. In 2006, Mangles *et al.* used an electron beam of energy up to 20 MeV for radiography of a solid material.[13] In 2010, Ramanathan *et al.* reported radiography of a cracked steel with a sub-millimeter resolution by using a quasi-monoenergetic electron beam with energies greater than 100 MeV.[14] More recently, in 2013, Bussolino *et al.* performed electron radiography of leaves, glass fibers and other samples, and a spatial resolution of approximately 60 μm was reached.[15]

To the best of our knowledge, no results have been reported on MeV electron beam radiography of plasma. In this Letter, we report numerical simulations on MeV electron beam scattering and transport in plasma, and the simulations are performed by a Monte Carlo (MC) code developed by ourselves. By choosing the electron's kinetic energy much greater than its energy loss inside plasma, an advantage of using such MeV electron beams for radiography is that inside the plasma the deflection of electrons by scattering is so small that the electrons transport in the plasma in approximately straight lines. As most of the plasma conditions in this work are close to fusion conditions, the incident electron energy greater than 100 MeV should be satisfied. Moreover, higher energy electrons are subjected to less deflections by the self-generated electromagnetic fields in plasma. Studying the transport and scattering of such a beam in plasma, we find a scaling law that may provide a new method of diagnosing the areal density of dense plasma by MeV electron radiography. In addition, the MeV electron radiography may also be applied for diagnosing plasma interfaces.

The MC model includes scattering processes and stopping power of electrons in plasma. In a regime of dense plasma, such as the compressed deuterium and tritium (DT) plasma in inertial confinement fusion (ICF), electrons essentially deposit their energy through collisions with plasma electrons and are scattered by both ions and electrons. As has been pointed out in Ref. [16] that for a very high density plasma close to fusion conditions, and also, as will be discussed in the following, by appropriately choosing the radiography geometry, the influence of self-generated electromagnetic fields in plasma on the electron scattering is expected to play a minor role. Therefore, for the present MC simulations, we employ the assumptions: (1) regardless of the interaction of electrons in the beam, (2) ignoring self-generated electromagnetic fields.

The relativistic differential cross section of electrons on plasma ions and electrons are expressed as[16]

$$\frac{d\sigma_{\mathrm{e-i}}}{d\Omega} = \left(\frac{Zr_0}{\gamma\beta^2}\right)^2 \frac{1}{4\sin^4(\theta/2)}\left(1-\beta^2\sin^2\frac{\theta}{2}\right) \cdot \left(\frac{\Lambda^2\sin^2(\theta/2)}{1+\Lambda^2\sin^2(\theta/2)}\right)^2, \tag{1}$$

$$\frac{d\sigma_{\mathrm{e-e}}}{d\Omega} = 4\left(\frac{r_0}{\gamma\beta^2}\right)^2 \cos\theta\left\{\frac{1}{\sin^4\theta} + \frac{(\gamma+1)^2}{4\cos^4\theta} + \frac{[(\gamma^2-1)/\gamma]^2}{[(\gamma-1)\sin^2\theta+2]^2} - \frac{(2\gamma-1)(\gamma+1)}{2\gamma^2\sin^2\theta\cos^2\theta}\right\} S(\gamma,\theta), \tag{2}$$

*Supported by the National Natural Science Foundation of China under Grant No 11375194.
**Corresponding author. Email: wang1@ustc.edu.cn
© 2016 Chinese Physical Society and IOP Publishing Ltd

and

$$S(\gamma,\theta)=\Big[\frac{(\Lambda/2)^2\sin^2\theta}{\frac{1}{2}(\gamma-1)\sin^2\theta+1+(\Lambda/2)^2\sin^2\theta}\Big]^2.$$

In these formulae m_e, e and c are the electron mass, the electron charge and the velocity of light in a vacuum, respectively, Z is the ion charge number, θ is the polar scattering angle, $\beta=v/c$ is the electron velocity normalized to the velocity of light in a vacuum, $r_0=e^2/m_ec^2$ is the classical electron radius, $\Lambda=4\pi\lambda_D/\lambda_{dB}$, $\lambda_{dB}=h/m_ec\beta\gamma$ is the de Broglie wavelength, $\lambda_D=\sqrt{k_BT/4\pi n_ee^2}$ is the Debye length, k_B is the Boltzmann constant, T is the plasma temperature, and n_e is the electron density of plasma. The above formulae are written in the laboratory frame with Gaussian units.

As shown in Refs. [16,17], the energy loss of relativistic electrons transporting in fully ionized plasma includes binary collisions with plasma electrons and plasma wave excitation. The stopping power for an electron with kinetic energy $E=(\gamma-1)m_ec^2$ due to the sum of these two factors is given by[16,17]

$$\Big(\frac{dE}{ds}\Big)_s=-\frac{2\pi r_0^2m_ec^2n_e}{\beta^2}\Big\{\ln\Big[\Big(\frac{E}{\hbar\omega_p}\Big)^2\frac{(\gamma+1)}{2\gamma^2}\Big]+1+\frac{1}{8}\Big(\frac{\gamma-1}{\gamma}\Big)^2-\Big(\frac{2\gamma-1}{\gamma^2}\Big)\ln 2\Big\},\quad(3)$$

where $\hbar=h/2\pi$ is the reduced Planck constant, $\omega_p=\sqrt{4\pi n_ee^2/m_e}$ is the electron plasma frequency.

Additionally, the stopping power due to radiation loss of charged particles in the material is given by[18]

$$\Big(\frac{dE}{ds}\Big)_{rad}=-4Z(Z+1)NEr_0^2\alpha\ln\frac{183}{Z^{1/3}},\quad(4)$$

where N is the plasma ion density, and α is the fine structure constant ($\sim 1/137$).

Finally, the total stopping power can be written as

$$\Big(\frac{dE}{ds}\Big)_t=\Big(\frac{dE}{ds}\Big)_s+\Big(\frac{dE}{ds}\Big)_{rad}.\quad(5)$$

In continuous slowing down approximation that is widely used in MC simulations, an electron at a given position moves with initial direction and energy. It moves along a straight path and continuously decelerates with the stopping power of Eq. (5) until it collides with the next particle of the plasma. For the incident electrons and the plasma parameters in this study, the radiation loss is less than the collisional loss, and as has been pointed out, the total energy loss is much less than the incident energy of electrons.

In our code, an electron's random tracking is generated by a classic method which is shown in the flow chart of Fig. 1. The tracking is described by a series of states. After the kth collision, the electron is on the state described by $\boldsymbol{r}_k$, $\hat{d}_k$, E_k, where $\boldsymbol{r}_k$ is the spatial coordinates of the kth collision, $\hat{d}_k$ is the direction cosine vector, and E_k is the kinetic energy of the electron. Before the next collision, the following steps are considered.

(i) Selecting collision object. Since several kinds of particles such as electrons and ions exist in the plasma, it is necessary to choose the collision object for the incident electron. The selection is a random process. The ith kind of particle to be selected takes the probability of $n_i\sigma_i/\sum n_i\sigma_i$, where n_i is the density of the ith kind of particle, and σ_i the interaction cross section of the incident electron to the ith kind of particle, which is obtained by integrating Eq. (1) or (2).

(ii) Sampling the length of the scatterer. For the kth scatterer, i.e., between the kth and the $(k+1)$th collision, the length of the scatterer is given by a sampling formula

$$s=-\lambda\ln\xi_1,\quad(6)$$

where ξ_1 is a random value in the range of $0\le\xi_1<1$, and λ is the mean free path expressed by $\lambda=1/\sum n_i\sigma_i$.

(iii) Sampling the polar and azimuthal angles. Each collision causes a deflection characterized by polar angle θ and azimuthal angle φ. For multiple scattering, the Gaussian distribution of the angle θ is determined by

$$f(\theta)=\frac{1}{\sqrt{2\pi\langle\Theta^2\rangle}}\exp\Big(-\frac{\theta^2}{2\langle\Theta^2\rangle}\Big),\quad(7)$$

where $\langle\Theta^2\rangle=s\sum_i n_i\int\theta^2(\frac{d\sigma}{d\Omega})_i d\Omega$ is the mean square angle of the Gaussian distribution, s is the length of scatterer, $(\frac{d\sigma}{d\Omega})_i$ is given by Eq. (1) or (2). The polar angle θ is extracted from the Gaussian sampling. As the scattering plane can be rotated randomly, we obtain the angle φ from a uniform distribution in 0–2π as $\varphi=2\pi\xi_2$, where ξ_2 is also a random number between 0 and 1. The direction vector $\hat{d}_{k+1}$ is deduced by performing a rotation of $\hat{d}_k$.

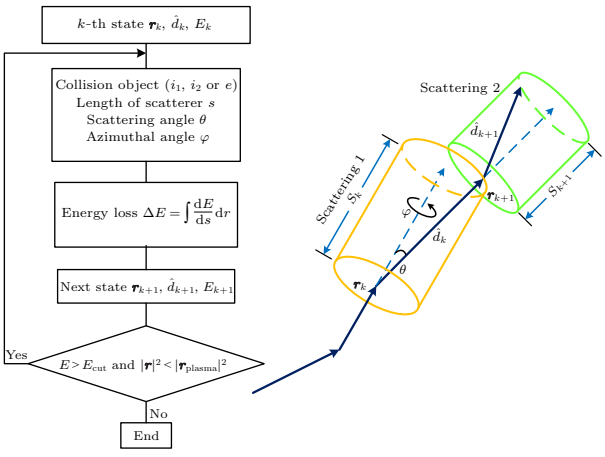

Fig. 1. (Color online) Flow chart and schematic diagram of scattering.

In the following we present some representative results obtained from the MC simulations. The results include the finding of a scaling law that may be applied in MeV electron radiography for areal density diagnosis. In addition, the electron scattering may be applied for plasma interface discrimination.

Firstly, the effect of the areal density, i.e., the product of target density and thickness, on the electron beam scattering angle is investigated. In ICF research, the product of mass density ρ and radius R, i.e., ρR, is defined as the constrained parameter which is also called the areal density. It is a critical physical parameter to characterize implosion,[19] and for ignition it requires $\rho R \geq 3\,\mathrm{g/cm^2}$. Diagnosing ρR becomes important while it is a difficult task in ICF experiments. Various methods such as neutron spectra,[20] proton radiography,[21] and x-ray imaging[22] have been proposed to diagnose ρR, while each has its limit. Here we explore a new diagnostic method using MeV electron beam scattering.

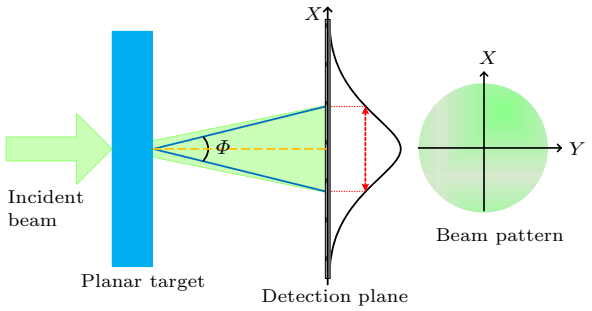

Fig. 2. (Color online) Schematic diagram of an electron beam radiographing a planar target. The electron beam pattern on the detection plane is schematically shown on the right.

For the first simulations, the target configuration is a planar target filled with uniform DT plasma, schematically shown in Fig. 2. A parallel electron beam of transversely narrow beam size is incident into and transmits through the plane target of different thickness. To investigate the angular spread of the electron beam after traversing the planar target, suppose that a detector is placed at 50 cm behind the target to record the beam pattern.

We compare the influence of plasma temperatures on the scattering. An electron beam with energy of 400 MeV and beam radius of 60 μm is incident into a planar target at temperature $T = 5\,\mathrm{keV}$ and at 10 keV, respectively. The target is 42.9 μm in thickness, its density is $700\,\mathrm{g/cm^3}$, and the corresponding areal density is $3.0\,\mathrm{g/cm^2}$. The plasma parameters such as densities, temperatures and areal densities are quite close to the high temperature, dense plasma under fusion conditions.[19] After traversing the plasma, the electron fluence distribution of the emergent beam on the detection plane is shown in Fig. 3(a). In the plot, the solid curve and the dashed curve signify the planar target with $T = 5\,\mathrm{keV}$ and 10 keV, respectively. It is seen that the difference between the peak values is 3.4% only, which indicates that the emergent beam profile is not sensitive to the plasma temperature.

Figure 3(a) shows that the fluence distribution is of Gaussian-profile shape. We define an angular width Φ, as visualized in Fig. 2, corresponding to the full width at half maximum (FWHM) of the beam profile on the detection plane. In this way, by fixing the incident electron beam energy at 400 MeV and the plasma temperature $T = 5\,\mathrm{keV}$, a series of angular widths are obtained by simulating the electron beam traversing targets of different areal densities, and the results are shown in Fig. 3(b), in which the circles and triangles signify the planar targets with $\rho = 700\,\mathrm{g/cm^3}$ and $143\,\mathrm{g/cm^3}$, respectively. It is seen that the angular widths increase monotonously with the increasing areal density. By fitting Φ versus ρR, a scaling relation $\Phi \propto \sqrt{\rho R}$ is found. Note that this scaling is dependent on the areal density rather than the single density or thickness of the target.

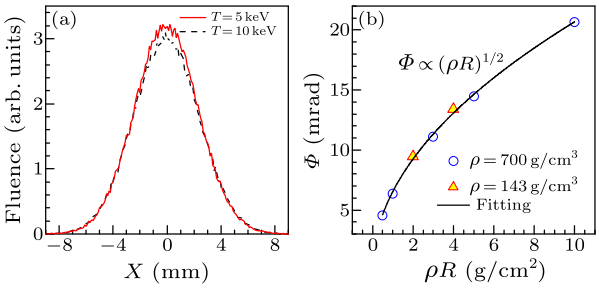

Fig. 3. (Color online) (a) Electron fluence distributions through the centerline of the beam pattern on the detection plane, and (b) the angular width as a function of the areal density.

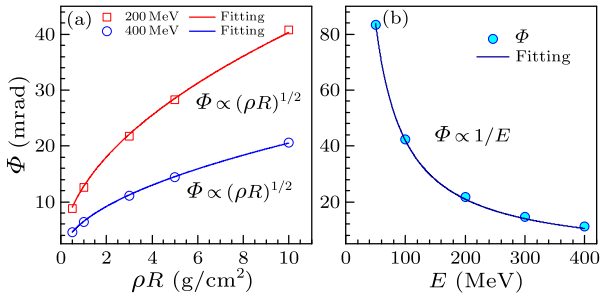

Fig. 4. (Color online) (a) The angular width as a function of the areal density for different incident electron energies, and (b) the angular width as a function of the incident electron energy for the areal density $\rho R = 3.0\,\mathrm{g/cm^2}$. The plasma temperature $T = 5\,\mathrm{keV}$ in both (a) and (b).

By changing the energy of the incident electron beam, the scaling law is still satisfied. Figure 4 shows the results for an incident beam of different energies. In general, Φ scales with ρR and E as

$$\Phi \propto \frac{\sqrt{\rho R}}{E}. \tag{8}$$

By fixing the incident energy, a scaling law can be written as

$$\rho R \propto \Phi^2. \tag{9}$$

Thus by measuring the angular width of the transmitted electron beam, ρR can be measured. This may provide a new method of diagnosing the areal density of plasma.

For realistic plasma such as in laser plasma interactions, there are essentially self-generated electromagnetic fields inside or around the plasma. Typically these fields are the axial electric field that is in parallel

to the plasma expansion due to the gradient of plasma pressure and the azimuthally toroidal magnetic field that is around the laser spot due to the non-collinear gradients of the plasma temperature and density.[23,24] The influences of the self-generated electromagnetic fields on the deflection of an electron beam are evaluated in the following.

Considering the magnetic field first, the deflection angle $\theta_{\rm M}$ for an electron's circular motion in a uniform magnetic field is

$$\theta_{\rm M} = \arcsin\left(\frac{\Delta x}{R_{\rm L}}\right), \tag{10}$$

where Δx is the width of the magnetic field region, and $R_{\rm L}$ is the electron's Larmor radius that reads

$$R_{\rm L} = \frac{m_{\rm e}c}{eB}\cdot\sqrt{\gamma^2-1}, \tag{11}$$

where B is the amplitude of the magnetic field. For a toroidal magnetic field around the laser spot, if face-on radiography is used, i.e., an electron beam is incident along the axial direction of the toroidal field, suppose a typical magnetic field $B\sim 1\,{\rm MG}$ or $100\,{\rm T}$[24] and $\Delta x\sim 100\,\mu{\rm m}$, then the electron beam with kinetic energies of 100, 200, 400 MeV, respectively, passing through the magnetic field region will be deflected by $\theta_{\rm M}\sim 29.8$, 14.9, and 7.5 mrad, respectively, which are of the same order in comparison with the beam divergence width Φ in Fig. 3 or 4. However, such a deflection is for the whole beam rather than causing the beam divergence. Even so, the whole-beam deflection by the toroidal magnetic field can be eliminated by appropriately choosing the radiography geometry. If one chooses side-on radiography, which was adopted to diagnose plasma electric fields in Ref. [23], the side-on incident electron beam passing through the toroidal magnetic field will be deflected twice oppositely by the reverse magnetic fields from the two sides of the toroidal magnetic field and the deflections will offset each other. Therefore the whole-beam deflection by the magnetic field would be eliminated. In this way one only needs to consider the influence of the plasma electric field.

Considering a uniform axial electric field of amplitude $E_{\rm a}$ over a region of width Δz, the deflection angle of an electron by the electric field can be expressed as

$$\theta_{\rm E} = \frac{eE_{\rm a}\cdot\Delta z}{(E+m_{\rm e}c^2)\beta^2}. \tag{12}$$

Suppose an electric field of $E_{\rm a}\sim 1.5\times 10^8\,{\rm V/m}$, which is typical in laser plasma interactions,[23] in a region of width $\Delta z\sim 100\,\mu{\rm m}$, then an electron beam with kinetic energies of 100, 200 and 400 MeV, respectively, passing through the electric field region will be deflected by $\theta_{\rm E}\sim 0.15$, 0.075, 0.038 mrad, respectively. These deflection angles are one order of magnitude smaller than the scattered angular width Φ. Thus the influence of electric fields can be ignored.

Therefore, by appropriately choosing the radiography geometry, such as by using side-on radiography, the influence of plasma self-generated electromagnetic fields could be ignored.

Next we expand the application of the scaling law in Eq. (9) by studying an MeV electron beam traversing a multilayer target. As shown in Fig. 5, for the multilayer target, the thickness of outer and inner layers are $L_1 = L_3 = 80.5\,\mu{\rm m}$ and $L_2 = 240\,\mu{\rm m}$, respectively. The inner is composed of heated, and the outer the colder, denser DT mixtures, which are used to simulate the dense plasma state for fast ignition, and the specific parameters are as follows.[25] For the inner layer, the temperature is set to be 5 keV and the density is $17.65\,{\rm g/cm^3}$. For the outer layers, the temperature is 1 keV and the density is $382.8\,{\rm g/cm^3}$. For these parameters, the calculated areal density of the target is $\rho R = 6.86\,{\rm g/cm^2}$.

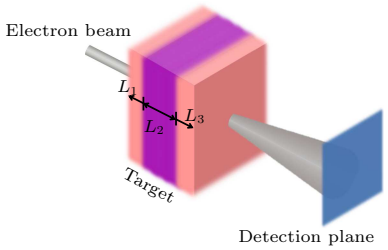

Fig. 5. (Color online) Schematic diagram of radiographing a multilayer target.

In the MC simulation, a fine electron beam with radius of 5 μm and energy of 400 MeV is incident into the target. The same as in the preceding part, the detector is placed at 50 cm behind the target. The simulation shows that the angular width of the emergent electron beam on the detection plane is 16.75 mrad, which, read from Fig. 3(b), corresponds to an areal density of $6.76\,{\rm g/cm^2}$. This value is in good agreement with the calculated one ($6.86\,{\rm g/cm^2}$), with difference less than 1.5%, which indicates that the scaling law in Eq. (9) can also be used to diagnose the areal density of a multilayer target.

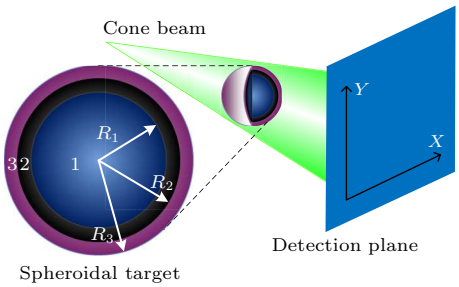

Fig. 6. (Color online) Schematic diagram of radiographing a spherical target.

Finally, we present a brief result showing that electron radiography may also be applied to diagnose an interface or a boundary of a target. Here a conical electron beam is used to radiograph a multilayered spherical target, as shown in Fig. 6. The layers marked by 1, 2, 3 are tenuous DT plasma, dense DT plasma and beryllium (Be) plasma, respectively.

We assume that the target temperature is 20 eV

and the D and T atoms are completely ionized while double electrons are ionized from the Be atoms at this temperature. The parameters of the spherical target in the simulation are summarized in Table 1.

Table 1. Parameters of the spherical target.

Region	Outer radius (cm)	Density (g/cm^3)
1	0.087	3×10^{-4}
2	0.095	0.25
3	0.108	1.9

In the simulation, the cone-shaped electron beam has a kinetic energy of 400 MeV and a divergence angle of 53 mrad for irradiating the target. The detector is located at 5 cm behind the target. Figure 7(a) shows the electron beam pattern on the detection plane. A line-out at $y = 0$ is shown in Fig. 7(b), in which I1, I2, I3 represent the three geometric projection positions of the interfaces between the vacuum and the Be layer, the Be layer and the dense DT layer, and the dense DT layer and tenuous DT plasma, respectively. The result shows that at the detection plane, the electron fluence distribution has modulations at the interfaces I1 and I2, which indicates that these interfaces can be discriminated by electron scattering. In fact, the scattering cross section between the electrons and plasma particles is several orders greater than that of x-ray Thomson scattering, which means that electron scattering will be an efficient way. The interface I3 between the dense DT layer and tenuous DT plasma cannot be discriminated, and this is due to the fact that the electrons transporting through the region of tenuous DT plasma will be further scattered in the outside layers, causing the scattering feature from the inside DT plasma to be smeared.

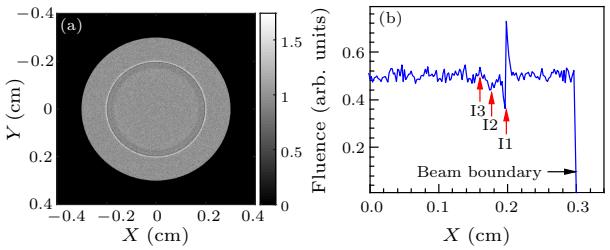

Fig. 7. (Color online) (a) Electron beam pattern on the detection plane, and (b) electron fluence through the centerline of (a).

In the simulations, it is found that with the detection plane moving farther away from the target, the modulation in the fluence distribution disappears gradually due to the deflection of the scattered electrons, and finally the fluence distribution becomes a Gaussian shape as shown in Fig. 3(a). This suggests that to see the modulation features, the detection plane should be close to the target and in such a case, an imaging system or a converter is preferred. For example, an image plate was used to acquire the angular distribution of fast electrons close to the target surface in laser plasma experiments,[26] which may be used as a detector in the present radiography.

In summary, an MC method has been developed to simulate MeV electron scattering in dense plasma targets. It is found that by plasma scattering of a collimated electron beam, the angular spread of the scattered beam is related to the areal density of the plasma by a scaling law $\rho R \propto \Phi^2$, which may provide a new method to diagnose the areal density of dense plasma. In addition, it is found that the MeV electron radiography may also be applied to diagnose the interfaces of a multilayered target. Therefore, MeV electron radiography will provide a new way for diagnosing dense plasma, which may provide new information or compensate for other diagnosis.

We thank Dr. Zhao B for his generous help and valuable discussion.

References

[1] Tajima T and Dawson J M 1979 *Phys. Rev. Lett.* **43** 267
[2] Mangles S P D, Murphy C D, Najmudin Z et al 2004 *Nature* **431** 535
[3] Geddes C G R, Toth Cs, Tilborg J V et al 2004 *Nature* **431** 538
[4] Faure J, Glinec Y, Pukhov A et al 2004 *Nature* **431** 541
[5] Kim H T, Pae K H, Cha H J et al 2013 *Phys. Rev. Lett.* **111** 165002
[6] Wang X, Zgadzaj R, Fazel N et al 2013 *Nat. Commun.* **4** 1988
[7] Zhu P, Zhang Z, Chen L et al 2010 *Appl. Phys. Lett.* **97** 211501
[8] Li J, Wang X, Chen Z et al 2010 *J. Appl. Phys.* **107** 083305
[9] Zhu P F, Zhang Z C, Chen L et al 2010 *Rev. Sci. Instrum.* **81** 103505
[10] Zhu P, Chen J, Li R et al 2013 *Appl. Phys. Lett.* **103** 231914
[11] Inoue S, Tokita S, Otani K et al 2011 *Appl. Phys. Lett.* **99** 031501
[12] Schumaker W, Nakanii N, McGuffey C et al 2013 *Phys. Rev. Lett.* **110** 015003
[13] Mangles S P D, Walton B R, Najmudin Z et al 2006 *Laser Part. Beams* **24** 185
[14] Ramanathan V, Banerjee S, Powers N et al 2010 *Phys. Rev. ST Accel. Beams* **13** 104701
[15] Bussolino G C, Faenov A, Giulietti A et al 2013 *J. Phys. D: Appl. Phys.* **46** 245501
[16] Atzeni S, Schiavi A and Davies J R 2009 *Plasma Phys. Control Fusion* **51** 015016
[17] Solodov A A and Betti R 2008 *Phys. Plasmas* **15** 042707
[18] Wang X L, Li C, Shao M and Chen H F 2009 *Particle Detection Techniques* (Hefei: USTC Press) p 27 (in Chinese)
[19] Atzeni S and Meyer-ter-vehn J 2004 *The Physics of Inertial Fusion* (Oxford: Oxford University Press) p 37
[20] Frenje J A, Casey D T, Li C K et al 2010 *Phys. Plasmas* **17** 056311
[21] Rygg J R, Séguin F H, Li C K et al 2008 *Science* **319** 1223
[22] Marshall F J, McKenty P W, Delettrez J A et al 2009 *Phys. Rev. Lett.* **102** 185004
[23] Li C K, Séguin F H, Frenje J A et al 2006 *Phys. Rev. Lett.* **97** 135003
[24] Cecchetti C A, Borghesi M, Fuchs J et al 2009 *Phys. Plasmas* **16** 043102
[25] Tabak M, Hammer J, Glinsky M E et al 1994 *Phys. Plasmas* **1** 1626
[26] Li Y T, Yuan X H, Xu M H et al 2006 *Phys. Rev. Lett.* **96** 165003